Dark and bright shock waves on oscillating backgrounds in a discrete nonlinear Schrödinger equation

V. V. Konotop [1,*] and M. Salerno [2,†]
[1]*Department of Physics, University of Madeira, Praça do Município, Funchal P-9000, Portugal and Center of Science and Technology of Madeira, Rua da Alfândega, 78-5°, P-9000 Portugal*
[2]*Department of Theoretical Physics, University of Salerno, I-84100 Salerno, Italy*
(Received 29 August 1996; revised manuscript received 7 February 1997)

Dark and bright shock waves on top of arbitrary oscillating backgrounds are investigated in a discrete version of the nonlinear Schrödinger equation. The existence of analytical curves in the parameter space corresponding to shock wave formation is established for arbitrary wave numbers k of the background radiation. The analysis is based on the small-amplitude approximation and is confirmed by direct numerical integrations of the system. [S1063-651X(97)02508-7]

PACS number(s): 03.20.+i, 11.10.Lm, 42.65.−k

I. INTRODUCTION

The general discrete nonlinear Schrödinger (GDNLS) equation

$$i\dot{q}_n+(1-\epsilon|q_n|^2)(q_{n-1}+q_{n+1}-2q_n)+2(\rho^2-|q_n|^2)q_n=0 \tag{1}$$

was introduced in Refs. [1–4] as a generalization of the simple tight-binding linear Schrödinger model for the dynamics of quasiparticles in a molecular crystal. This model naturally appears in the theory of intrinsic localized modes [5] and describes Frenkel excitons in a one-dimensional chain of two-level atoms with energy transfer by an exchange interaction [6,7]. In order to study Eq. (1) in a general context, q_n is regarded as the displacement field, ϵ is a deformation parameter, which in the present paper will be considered positive $(0<\epsilon<1)$, ρ is a constant that is associated with the amplitude of q_n at infinity,

$$\lim_{n\to\pm\infty} q_n=\rho\exp\{-i(\omega t-kn\pm\varphi)\}, \tag{2}$$

and

$$\omega\equiv\omega(k)=4(1-\epsilon\rho^2)\sin^2\frac{k}{2} \tag{3}$$

represents the dispersion relation of a plane wave with amplitude ρ, wave number k (taken in the first Brillouin zone $[-\pi,\pi]$), and phase $\varphi\in[0,\pi]$. From a mathematical point of view Eq. (1) represents a norm-preserving deformation of the diagonal (on-site) discretization of the nonlinear Schrödinger equation (DNLS), which reduces for $\epsilon=1$ to the integrable Ablowitz-Ladik model [8] and for $\epsilon=0$ to the nonintegrable DNLS system. The presence of the deformation parameter in the model allows one to study the interplay between on-site–intersite interactions as well as integrability-nonintegrability and discrete-continuum properties as done in Refs. [4,9–13]. The aim of the present paper is to show the existence of shock waves in the GDNLS system moving on backgrounds with arbitrary wave numbers in the Brillouin zone (BZ). These shock waves are in some aspects similar to those found in other integrable [14–17] and nonintegrable models [18,19]. In particular, their profiles can be considered as consisting of three qualitatively different components: a smooth part, which at the initial stages of the evolution corresponds to the rear or to the front (in some cases represented below); a rapidly varying ''front,'' and a train of solitonlike pulses. On the other hand, the shock waves we discuss also possess a number of different features. First, our model allows the existence of both *bright* and *dark shock waves*. Second, the evolution of a shock wave (in the long-wavelength limit) is described by the simple first-order equation $c_t+cc_x=0$ [20], which is different from the one governing shocks in other discrete systems [19]. Using this equation, we can predict the breaking time of the wave in excellent agreement with numerical results. Third, there exist two branch lines in parameter space on which shock waves propagate with different velocities and are characterized by different effective nonlinearities. Fourth, the mutual location of the components of the waves with respect to the wave front depends on the problem parameters. Finally, the shock waves reported here, in contrast with the ones observed in other nonlinear lattices, develop from smooth initial (bright or dark) profiles [13] and disappear in the integrable limit of the model.

The organization of the paper is as follows. In Sec. II we develop the theory of the shock waves based both on linear analysis and on multiscale expansion. In Sec. III we provide a numerical investigation of the shock wave dynamics and in Sec. IV we discuss the numerical results on the basis of our analytical considerations. Finally, the main results of the paper are briefly summarized in Sec. V.

II. SHOCK WAVES IN THE SMALL-AMPLITUDE LIMIT

In order to describe shock wave formation in the GDNLS system it is more convenient to perform the change of variables

*Also at Center of Mathematical Sciences, University of Madeira, Praça do Município, Funchal P-9000 Portugal.

†Also at Istituto Nazionale di Fisica della Materia, Unitá di Salerno, Salerno, Italy.

$$\psi_n = q_n \exp(i\omega t - ikn). \tag{4}$$

Equation (1) then becomes

$$\begin{aligned} & i\dot{\psi}_n + \cos(k)(1-\epsilon|\psi_n|^2)(\psi_{n+1}+\psi_{n-1}-2\psi_n) \\ & + i\sin(k)(1-\epsilon|\psi_n|^2)(\psi_{n+1}-\psi_{n-1}) \\ & + 2(1-\epsilon+\epsilon\cos k)\psi_n(\rho^2-|\psi_n|^2)=0, \end{aligned} \tag{5}$$

subject to the boundary condition

$$\lim_{n\to\pm\infty} \psi_n = \rho \exp(\pm i\varphi). \tag{6}$$

For $\epsilon=1$ Eq. (5) is recognized as the discrete Hirota (DH) equation, which is integrable by means of the inverse scattering technique [21] and has exact dark multisoliton solutions [7]. In the following sections we study the linear excitation and the small-amplitude limit of Eq. (5), which in the following we refer to as the deformable discrete Hirota (DDH) equation.

A. Linear analysis

Let us start our investigation with the analysis of the linear excitations of Eq. (5). This will provide information both on the stability of the background field and on the existence of regions of the parameter space where shock waves can be observed. To this end we consider the solution of Eq. (5) in the form $\psi_n=\rho+\phi_n$ where $|\phi_n|\ll\rho$. By expanding Eq. (5) with respect to ϕ_n, we obtain to first order the dispersion relation of linear waves

$$\begin{aligned} \Omega_{\pm}(K) = {} & 2\sin k(1-\epsilon\rho^2)\sin K \pm 4\sqrt{\cos k(1-\epsilon\rho^2)}\sin(K/2) \\ & \times[\cos k(1-\epsilon\rho^2)\sin^2(K/2) \\ & + (1-\epsilon+\epsilon\cos k)\rho^2]^{1/2}. \end{aligned} \tag{7}$$

From Eq. (7) it follows that the background is modulationally stable for $\epsilon\rho^2<1$ and $k\in[-\pi,k_0-\pi]\cup-\pi/2, \pi/2\cup[\pi-k_0,\pi]$ or for $\epsilon\rho^2>1$ and $k\in[k_0-\pi,\pi/2]\cup[\pi/2,\pi-k_0]$, where $k_0=\cos^{-1}(\epsilon^{-1}-1)$ at $\epsilon>1/2$ and $k_0=0$ otherwise. In particular, we have that in the integrable limit ($\epsilon=1$) only backgrounds with $\epsilon\rho^2<1$ are stable. Below we shall restrict our consideration to only these regions of stability. It is worth remarking that the dispersion relation has two branches and the expansion of the group velocity $V_{\pm}=d\Omega_{\pm}/dK$ at small K gives

$$\begin{aligned} V_{\pm} = c_{\pm} - \Bigg[& \sin k \mp \frac{\cos k}{4}\left(\frac{3}{\rho}\sqrt{\frac{(1-\epsilon\rho^2)\cos k}{1-\epsilon+\epsilon\cos k}}\right. \\ & \left. - \rho\sqrt{\frac{1-\epsilon+\epsilon\cos k}{(1-\epsilon\rho^2)\cos k}}\right)\Bigg]\frac{1-\epsilon\rho^2}{3}K^2 + O(K^4), \end{aligned} \tag{8}$$

where

$$c_{\pm} = 2\sin k(1-\epsilon\rho^2) \pm 2\rho\sqrt{\cos k(1-\epsilon\rho^2)(1-\epsilon+\epsilon\cos k)} \tag{9}$$

is the group velocity of the harmonic $K=0$. Note that $c_{\pm}=0$ at $\rho=1/\sqrt{\epsilon}$. This amplitude corresponds to singular points that split the chain in a sequence of independent segments [13], implying that no energy transfer along the chain is possible at such an amplitude of the background. From a physical point of view one expects shock waves to occur when the nonlinearity dominates the group velocity dispersion [note that if the nonlinearity is weak, one can use expansion (8) to calculate the dispersion as a function of the parameters]. Obviously, the weakest dispersion appears in the case when the factor of K^2 in Eq. (8) is zero, i.e., when

$$4\sin k = \pm\cos k\left(\frac{3}{\rho}\sqrt{\frac{(1-\epsilon\rho^2)\cos k}{1-\epsilon+\epsilon\cos k}} - \rho\sqrt{\frac{1-\epsilon+\epsilon\cos k}{(1-\epsilon\rho^2)\cos k}}\right). \tag{10}$$

From this condition it is clear that waves moving on different backgrounds display shocks on different curves in the parameter space $\rho-\epsilon$. In Figs. 1(a) and 1(b) we have reported the curves $\epsilon(\rho,k)$ obtained from Eq. (10) for different values of k, i.e.,

$$\epsilon_{\pm} = \frac{1}{\rho^2}\left[\frac{9\cos^3 k - \rho^2[f_{\pm}(k)]^2}{9\cos^3 k - (1-\cos k)[f_{\pm}(k)]^2}\right], \tag{11}$$

where

$$f_{\pm}(k) = 2\sin k \pm \sqrt{\sin^2 k + 3}. \tag{12}$$

We remark that at $k=0$ (uniform backgrounds), Eq. (11) reproduces the simple relation $\epsilon=\rho^{-2}-3^{-1}$ obtained in Ref. [13]. Moreover, for $k\neq 0$ (in the case $\epsilon\rho^2<1$) and $k\neq\pi$ (in the case $\epsilon\rho^2>1$) splitting of the curves occurs and two branches appear. The most interesting region from a physical point of view is that defined by the condition $\epsilon\rho^2<1$. For $\epsilon\rho^2>1$, however, the dynamics governed by the DDH equation also displays some interesting features. One of them is seen in Fig. 1(b): for each k there exists a cutoff value of ϵ represented by the point where two branches with the same k intersect. One can readily check that these intersection points occur at $\epsilon_{cut}=(1-\cos k)^{-1}$, this being just the threshold value for linear stability. We expect, therefore, that on the part of the curves of Fig. 1(b) above ϵ_{cut}, shock waves should not exist because of the modulational instability of the background.

B. Small-amplitude expansion

The equation governing shock wave dynamics (at the earlier stages of their evolution) can be obtained in the small-amplitude limit by following the same analysis of Ref. [13]. Here we generalize the corresponding expansions to the case of arbitrary k in the BZ. To this end we represent $\psi_n=(\rho+\mu^2 a)\exp(-i\mu\phi)$, where $a=a_0+\mu^2 a_1$, and $\phi=\phi_0+\mu^2\phi_1$, where μ is a small parameter ($\mu\ll 1$). By introducing a spatial variable $X=\mu n$, which is treated as a continuum variable, as well as ''slow'' times $T=\mu t$ and $\tau=\mu^3 t$ (regarded as continuous) we derive the expansion with respect to the small parameters and arrive, in the lowest orders in μ, at the equations for the phase ϕ_0, and amplitude a_0

$$\begin{aligned} & \frac{\partial^2\phi_0}{\partial T^2} + 2\gamma\frac{\partial^2\phi_0}{\partial T\partial X} - \beta\frac{\partial^2\phi_0}{\partial X^2} = 0, \\ & \frac{\partial a_0}{\partial T} + \gamma\frac{\partial a_0}{\partial X} = \frac{\gamma}{2\ \tanh}\frac{\partial^2\phi_0}{\partial X^2}, \end{aligned} \tag{13}$$

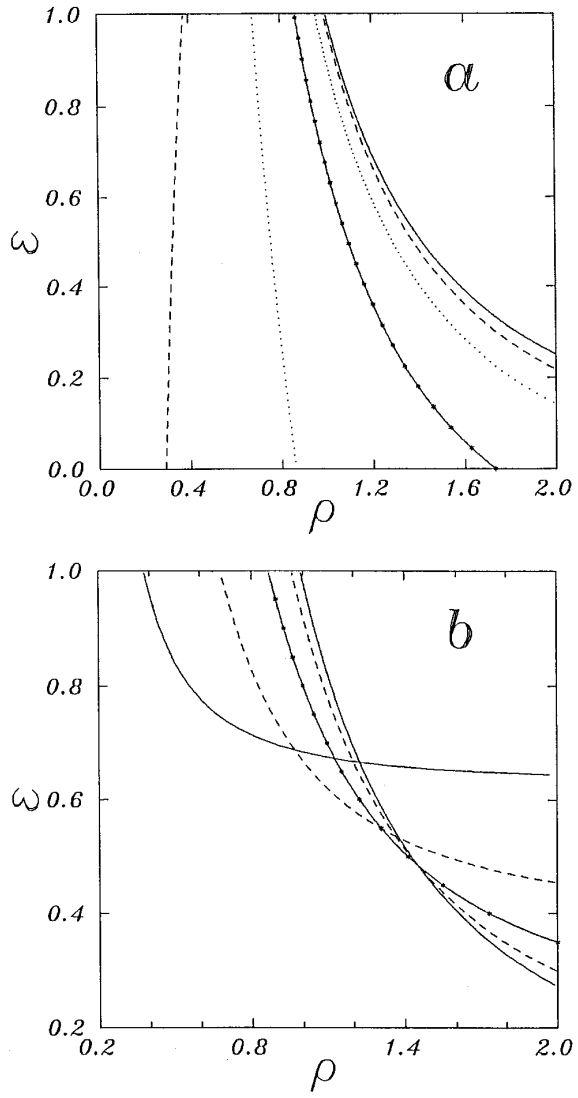

FIG. 1. (a) Shock wave formation curves $\epsilon_{\pm}$ in Eq. (11) plotted for several values of the background wave number $0 \leqslant k \leqslant \pi/2$. The continuous curve with stars refers to $k=0$, the dashed lines to $k=\pi/3$, the dotted ones to $k=\pi/6$, and the continuous one to $k=\pi/2$. The curves on the left of the $k=0$ curve refer to the positive branch ϵ_{+}, while those on the right refer to the negative one. The curve $\epsilon_{+}(k=\pi/2)$ is not seen because it overlaps with the vertical axis ($\rho=0$). (b) Same as in (a), but for wave numbers $\pi/2 \leqslant k \leqslant \pi$. The continuous curve with stars refers to $k=\pi$, the dashed lines to $k=\frac{5}{6}\pi$, and the continuous ones to $k=\frac{2}{3}\pi$. The curves starting at $\epsilon=1$ on the left of the $k=\pi$ curve refer to the positive branch ϵ_{+}, while those starting on the right refer to the negative one. The intersection point of two branch lines of the same type gives the threshold for the modulational stability of the background.

where

$$\beta = 4(1-\epsilon\rho^2)[\rho^2 \cos k - \sin^2 k + \epsilon\rho^2(1-\cos k)] \quad (14)$$

and

$$\gamma = 2(1-\epsilon\rho^2)\sin k. \quad (15)$$

The general solution of Eq. (13) is represented by two dispersionless waves propagating with velocities $c_{\pm}$ given by Eq. (9) (note that $c_{\pm}$ can be rewritten in the form $c_{\pm}=\gamma \pm \sqrt{\gamma^2+\beta}$). Introducing a running variable $\xi_{\pm}=X-c_{\pm}T$ and looking at solutions of the form $\phi_0 \equiv \phi_0(\xi_{\pm}, \tau)$, we can express a_0 through ϕ_0 as

$$a_0 = a_{\pm} = \mp \frac{1}{2\rho}\sqrt{\frac{(1-\epsilon\rho^2)\cos k}{1-\epsilon+\epsilon\cos k}}\frac{\partial \phi_0}{\partial \xi_{\pm}}. \quad (16)$$

By taking into account Eq. (16) and collecting the terms of the order of μ^4 and μ^5, we finally arrive at a system of equations whose compatibility condition is expressed as

$$\frac{\partial a_{\pm}}{\partial \tau} - b_1^{(\pm)}(k) a_{\pm}\frac{\partial a_{\pm}}{\partial \xi_{\pm}} - b_2^{(\pm)}(k)\frac{\partial a_{\pm}}{\partial \xi_{\pm}^3} = 0, \quad (17)$$

where the coefficients $b_{1,2}(k)$ are given by

$$b_1^{(\pm)}(k) = 2\rho^2 \sin k\left(4\epsilon + \frac{1-\epsilon}{\cos k}\right) \mp 2\rho\sqrt{\cos k \frac{1-\epsilon+\epsilon\cos k}{1-\epsilon\rho^2}} \times (3-4\epsilon\rho^2), \quad (18)$$

$$b_2^{(\pm)}(k) = \frac{1-\epsilon\rho^2}{12}\left[-4\sin k \pm \cos k\left(\frac{3}{\rho}\sqrt{\frac{(1-\epsilon\rho^2)\cos k}{1-\epsilon+\epsilon\cos k}} - \rho\sqrt{\frac{1-\epsilon+\epsilon\cos k}{(1-\epsilon\rho^2)\cos k}}\right)\right]. \quad (19)$$

Equation (17) is just a Korteweg–de Vries (KdV) equation for $a_{\pm}$ with respect to the space variable $\xi_{\pm}$. For $b_2^{(\pm)}(k)=0$ Eq. (17) transforms to the well-known equation [20]

$$\frac{\partial a_{\pm}}{\partial \tau} - b_1^{(\pm)}(k) a_{\pm}\frac{\partial a_{\pm}}{\partial \xi_{\pm}} = 0 \quad (20)$$

governing shock waves. It is worth noting that the condition $b_2^{(\pm)}(k)=0$ is nothing but Eq. (11) obtained before using qualitative arguments. We also remark that the approach of Eq. (17) is more general since it allows one to estimate also the effective nonlinearity. In particular, at $\epsilon=1$ one has that $b_1^{(\pm)}(k)=0$ if $b_2^{(\pm)}(k)=0$ and hence shock waves cannot exist. This result is predictable since $\epsilon=1$ corresponds to the exactly integrable discrete Hirota equation, which does have dark soliton solutions [7] but not shock waves. From Eq. (18) it also follows that in the nonintegrable case ($\epsilon \neq 1$) $b_1(\pi/2)=\infty$. Formally, this means that the point $k=\pi/2$ at $\epsilon \neq 1$ is out of the applicability region of the small-amplitude approximation. Since a wave packet with the spectrum centered at $k=\pi/2$ has harmonics with $k>\pi/2$, the background becomes unstable as $k \to \pi/2+0$ (see the linear analysis above).

III. NUMERICAL ANALYSIS

To check the above analytical results we have numerically integrated Eq. (1) using a fifth-order adaptive step size Runge-Kutta algorithm. The chain was taken to be long enough to ignore boundary conditions and the initial condition was taken as

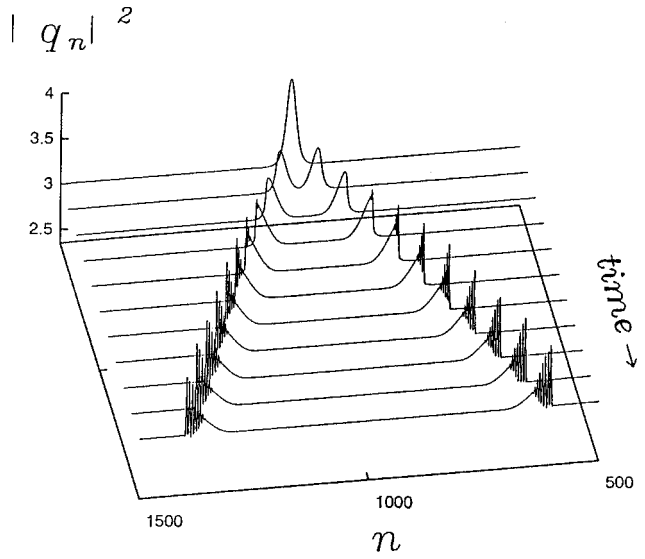

FIG. 2. Evolution of bright shocks against nonzero background with $k=0$, $\rho=\sqrt{3}$, and $\epsilon=0$.

$$q_n=\rho e^{i(kn+\phi)}\left(1\pm\frac{s}{\cosh[(n-n_0)]^2}\right), \tag{21}$$

i.e., a bell-shaped profile on top of an oscillating background of amplitude ρ, wave number k, and frequency ω [given by Eq. (3)]. We investigate first the case of shock waves on uniform backgrounds $(k=0)$ for which the two branch curves $\epsilon_{\pm}$ in parameter space coincide [see Eq. (11)]. We examine successively the case of shock waves on arbitrary backgrounds.

In Fig. 2 we report the time evolution of a bright [the plus sign in Eq. (21)] initial profile of amplitude $s=2$ on a background characterized by $k=0$ and $\rho=\sqrt{3}$. We see that the initial profile splits into two smooth profiles moving in opposite directions, both bending in the direction of propagation and developing, after a certain time, oscillations starting from the top. We define the breaking time t_B of the wave as the time at which the oscillations first appear on the profiles. An estimate of this time for an initial profile $q=f(\xi)$ can be obtained from the continuous equation (20) as $t_B=-[F'(\xi_B)]^{-1}$, where $F(\xi)=a(f(\xi))$ and ξ_B is the value of the characteristic for which $F'(\xi)<0$ and $|F(\xi)|$ is maximum. Using Eq. (20), we readily obtain

$$t_B=\frac{\sqrt{3}}{2s\nu^2(4\rho^2-3)}\frac{\cosh^2(\nu\xi_B)}{\tanh(\nu\xi_B)}, \tag{22}$$

with $\sinh\nu\xi_B=\sinh^{-1}(1/2)$. In Fig. 3 we report the breaking time as obtained from Eq. (22) (continuous curve) in comparison with direct numerical experiments (dotted squares). We see that there is good agreement between the theory and the numerical analysis up to times of the order of the breaking time. In Fig. 4 we report the profile of one of the shocks of Fig. 2 after an evolution time $t=2400$. From this figure it is clear that the oscillation that develops behind the bright shock generates, after a long time, a train of solitons with the solitons in the front widely spaced with respect to the ones at the end. We note that the two leading solitons in Fig. 4 are more closely spaced than the following leading ones, this

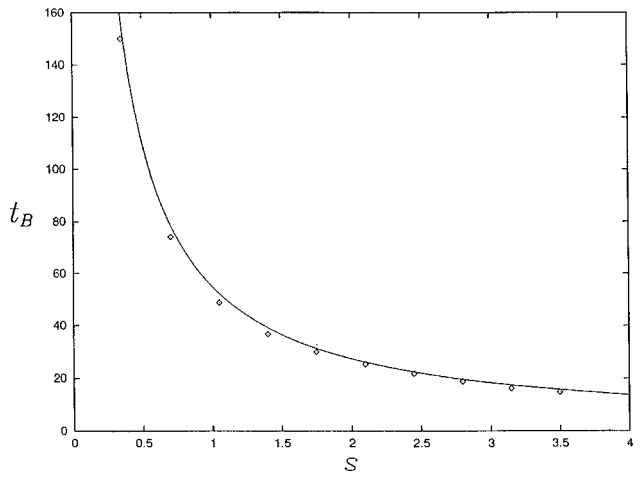

FIG. 3. Breaking time versus the amplitude of the shock for the same parameter values as in Fig. 2. The continuous curve refers to Eq. (20), while the dotted squares are experimental points.

being reminiscent of the shock wave front formed at earlier times. By reducing the amplitude of the initial profile the two leading solitons are found to be very close for long times (they separate very slowly with respect to each other), while the rest of the solitons in the train arrange in a triangular shaped configuration. Moreover, as the amplitude of the initial profile is reduced, the time required to decompose a bright shock into solitons increases, but the scenario observed is just the same. In the case of a dark shock the picture is quite different since complicated oscillations behind the shock front develop and the soliton component of the wave becomes evident only when approaching the integrable limit. To show this we report in Fig. 5 the time evolution of a dark [the minus sign in Eq. (21)] initial profile on a background characterized by $k=0$ with $\rho=\sqrt{3}$ and ϵ derived from Eq. (11). We see that there is a sharp transition between the front of the wave profile and the background radiation that develop in the rear. By increasing the value of ϵ along the corresponding curve in Fig. 1(a) it becomes evident that a dark shock is characterized by three regions: the wave front, which is a smooth profile (ending with a discontinuity); the middle, which can be interpreted in terms of a soliton train (see below); and the tail, which appears as back-

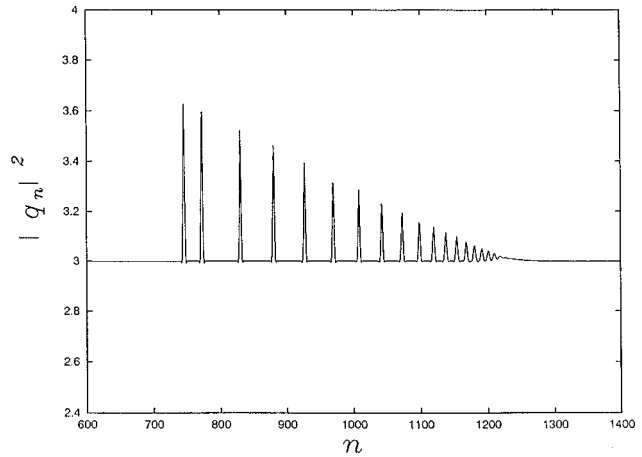

FIG. 4. Profile of one of the bright shocks of Fig. 2 after an evolution time of 2400.

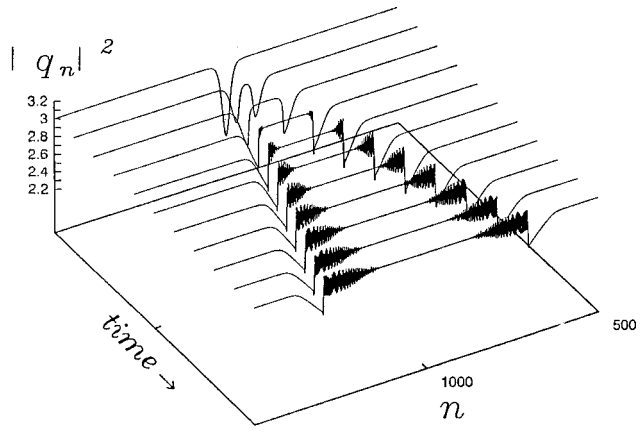

FIG. 5. Evolution of dark shocks against nonzero background with $k=0$, $\rho=\sqrt{3}$, and $\epsilon=0$.

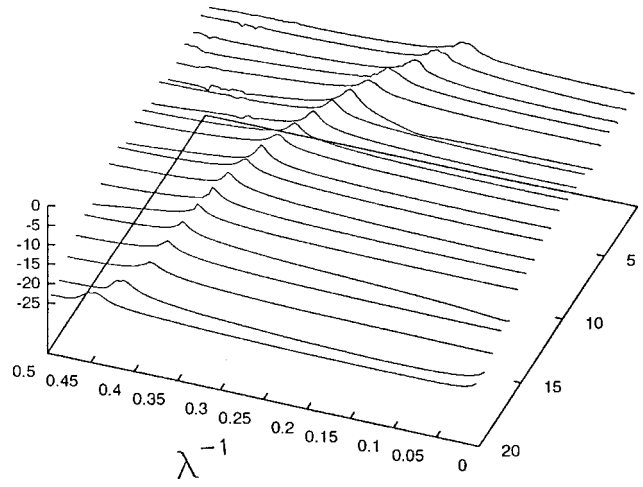

FIG. 7. Power spectrum analysis of the oscillating part (points) of the dark shock in Fig. 6. The signal is divided in 20 consecutive intervals of 256 points each starting from the head. The logarithm of the power spectrum is reported on the vertical axis versus the reciprocal of the wavelength for each interval.

ground radiation. This is clearly seen from Fig. 6, where the profile of a dark pulse is reported after an evolution time $t=7200$ for parameter values $k=0$, $\rho=1$, and $\epsilon=\frac{2}{3}$. To clearly distinguish the front, the middle, and the oscillating tail of the shock we use different line thicknesses for the front and the middle part, while the tail is plotted just by points. Analyzing the oscillating part of the profile in Fig. 6 we find that its harmonic content changes as one moves towards the far end of the wave. This is clearly seen in Fig. 7, where the power spectrum of the oscillating part of the profile in Fig. 6 is reported. The signal is spliced into 20 consecutive intervals of 256 points and for each interval the spectrum is displayed. We see that at the end of the tail the wavelength of the signal approaches the limiting value of 2 (see the lowest curve in Fig. 7), i.e., the wave number k of the radiation approaches the edge of the Brillouin zone ($k=\pi$). Moving towards the integrable limit, we find that the tail radiation is reduced while the middle region is enhanced and its interpretation in terms of a train of solitons becomes more evident. This is shown in Fig. 8, in which a dark shock profile at time $t=2400$, for parameter values $k=0$, $\epsilon=0.95$, and ρ derived from Eq. (11), is reported. At $\epsilon=1$ (the DH limit) we find that the background radiation in the tail completely disappears and the shock wave degenerates into a triangular-shaped train of solitons. Thus, at the deformation parameter close to 1, the middle part of the shock wave can be correctly interpreted as a train of dark solitons. The above behavior generalizes to nonuniform backgrounds with arbitrary wave numbers in the BZ. In particular, in Fig. 9 we report the profile of a dark shock wave after an evolution time $t=1000$ moving on a background characterized by $k=\pi/6$ and $\epsilon=0.3$ with ρ obtained from curve ϵ_+ in Eq. (11). By increasing the value of ϵ along the curve ϵ_+ (i.e., moving towards the integrable DH limit) we observe the same phenomena described in the $k=0$ case. These results are quite general and hold true for other positive ϵ branches of Fig. 1. On the other hand, the behavior of a dark shock is different for parameter values on the negative ϵ branches. This is evident from Fig. 10, where the profile of a dark shock wave developing from an initial profile of amplitude $s=2.1$ on a background with wave number $k=\pi/6$ is reported for $\epsilon=0.3$ and ρ obtained from the corresponding curve ϵ_- in Fig. 1(a). It is remarkable that the wave develops a rectangular wave front followed by a train of solitons with background radiation at the end (a possible interpretation of

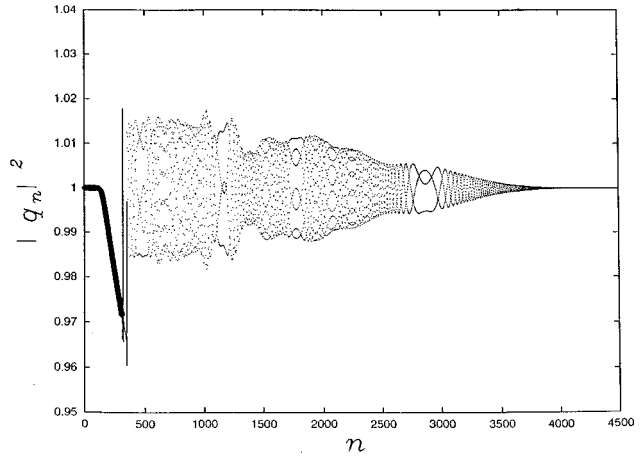

FIG. 6. Profile of one of the dark shocks of Fig. 5 after a time of 7200.

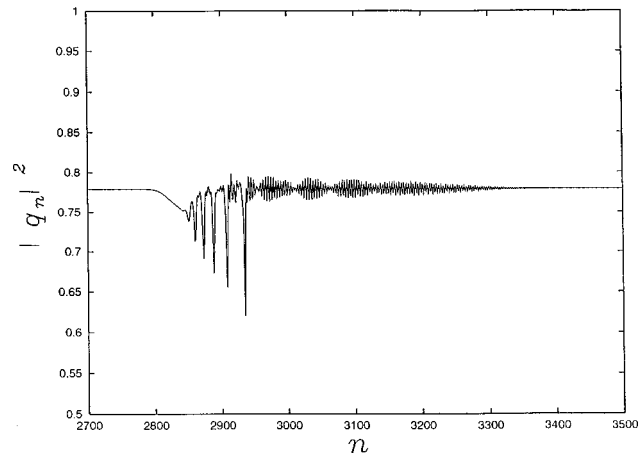

FIG. 8. Same as in Fig. 6, but for $\epsilon=0.95$ and ρ derived from Eq. (11). The evolution time is 2400.

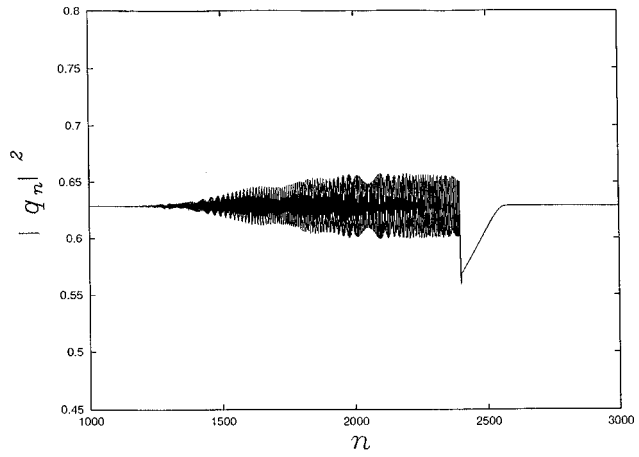

FIG. 9. Dark shock profile after an evolution time $t=1000$, for parameter values $\epsilon=0.3$, $k=\pi/6$, and ρ derived from the positive branch curve $k=\pi/6$ of Fig. 1(a).

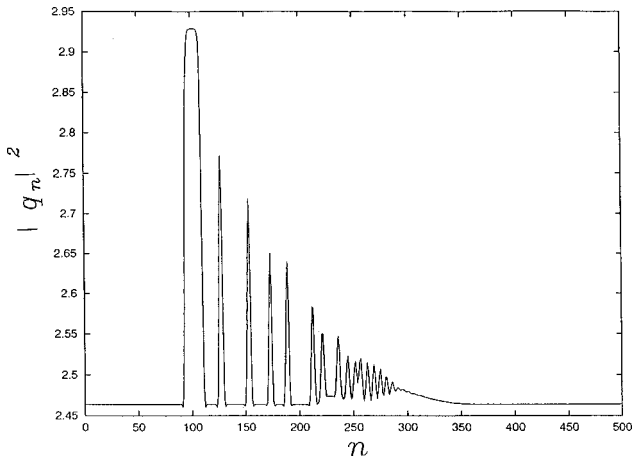

FIG. 11. Bright shock profile for parameter values $\epsilon=0.3$, $k=\pi/6$, and ρ derived from the corresponding negative branch curve of Fig. 1(a). The amplitude of the initial profile is $s=1.26$ and the total evolution time is $t=2400$.

the square wave front in terms of closely spaced solitons bunched together is quite appealing). A similar phenomenon is observed also in the case of bright shocks on negative ϵ branches. This can be seen from Fig. 11, where the profile of a bright shock on the background with $k=\pi/6$, $\epsilon=0.3$, and ρ determined from the curve ϵ_- in Eq. (11) is reported. Note that in this case the square wave front is more ''rounded'' than the one in Fig. 10. This depends on the amplitude (energy) of the initial profile, which in this case is smaller [$s=1.2$ instead of $s=2.1$ in Eq. (21)]. As we increase the amplitude of the initial profile the leading square wave becomes sharper, but the phenomenon also becomes more involved (more shock waves, usually of different kinds, may be created). This is shown in Fig. 12, where the time evolution of an initial profile of amplitude $s=2.2$ is reported. We see that the initial profile splits into two waves moving in opposite directions. The profile of the wave moving on the right is reported in Fig. 13 after an evolution time $t=3600$. From this figure it is evident that there are really two shock waves, one bright and the other dark. The inset of Fig. 13 shows the wave fronts of the two shock waves plotted by points (diamonds) joined by lines from which the sharpness of the leading square wave is clearly seen. The other small wave moving on the left of Fig. 12 is also found in the time evolution of an initial bright profile for parameter values taken on the positive branches ϵ_+ in Eq. (11). We have investigated also the behavior of shocks on curves of Fig. 1(b), i.e., for wave vectors $\pi>k>\pi/2$. In this case we have that, in agreement with our stability analysis, shock wave formation is possible only on the part of the curves that satisfy the stability criterion derived in Sec. II B.

Finally, we have investigated scattering processes of shock waves of different types. Quite surprisingly, we find that the shock profiles, like solitons, are well preserved under scattering processes as shown in Fig. 14 for the case of a bright-dark shock collision. This result further confirms the existence of a strong solitonic component in the shock wave described above (details of this phenomenon will be given elsewhere [22]).

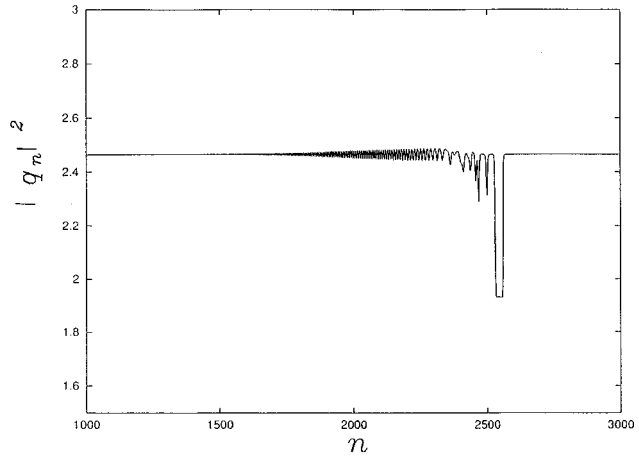

FIG. 10. Profile of a dark shock of the DDH equation for parameter values $\epsilon=0.3$, $k=\pi/6$, and ρ derived from the negative branch curve $k=\pi/6$ of Fig. 1(a). The total evolution time is $t=1800$.

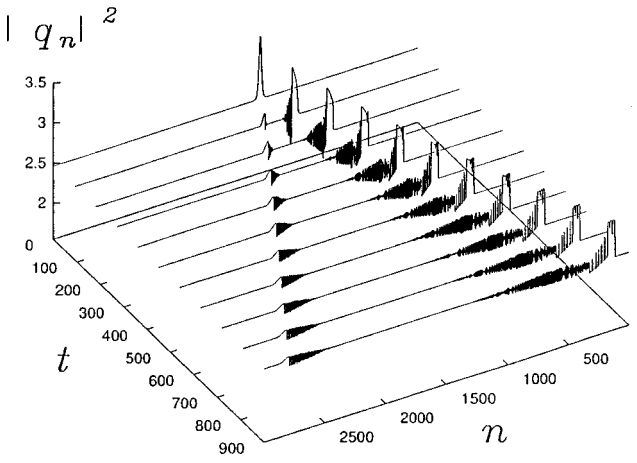

FIG. 12. Time evolution of an initial bright profile of the DDH equation for parameter values $\epsilon=0.3$, $k=\pi/6$, and ρ derived from the corresponding negative branch curve of Fig. 1(a). The amplitude of the initial profile is $s=2.1$.

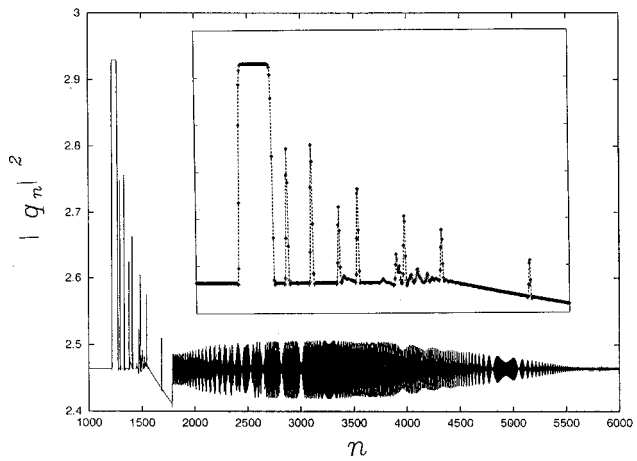

FIG. 13. Right profile of Fig. 12 plotted after an evolution time $t=3600$. The inset shows the leading part of the profile plotted by points (diamonds) joined by lines.

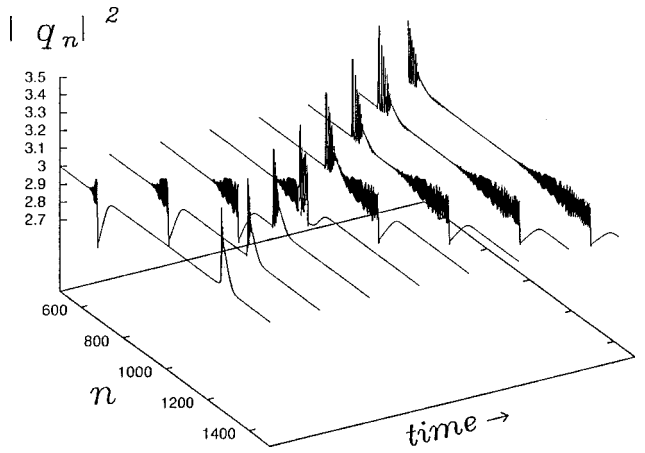

FIG. 14. Dark-bright shock scattering for parameter values as in Fig. 2.

IV. DISCUSSION

In order to interpret our numerical results and in particular the relatively stable single pulses originated by shocks, we have used the soliton terminology. Since for generic parameter values the model is not integrable, this point requires further explanation. To this end we note from Eq. (16) that the phase mismatch between neighboring particles depends on the amplitude of the wave. This implies that the change of the amplitude during the shock evolution results in a change of the central wave vector of the wave packet (this is also confirmed by our simulations). In turn, this means that localized modes associated with shocks are out of the regions of the spectral space that corresponds to shock waves, i.e., they cannot produce secondary shocks. On the other hand, out of these regions (however, not too far), the pulses are described by the KdV equation (10). If the wave number is changed significantly, then the provided expansion is not applicable anymore, but for Ω not too small it is known that any conservative discrete system possesses an envelope soliton (in some approximation of course) [23]. Such solutions are quite stable and propagate along the chain without distortion for long times. Their amplitude, a small parameter, multiplied by the width gives a quantity of order one. As is clearly seen from the inset of Fig. 13, localized pulses in the numerical experiments have amplitudes of order 0.1–0.3 and involve about ten sites, i.e., have characteristics typical for envelope solitons. A more detailed analysis of this phenomenon, however, requires further analytical investigations. Another important feature observed in the dynamics of the shock waves described above is the alternation of the location of the shock front with respect to the characteristic $n=V_{\pm}t$. A preliminary explanation of it can be obtained by observing that the coefficient $b_1^{\pm}(k)$ subject to the condition (11) takes the form

$$b_1^{(\pm)}(k)=18(1-\epsilon)\frac{\cos^2 k[\sin k\mp|f_{\pm}(k)|]}{\epsilon[9\cos^3 k-(1-\cos k)f_{\pm}^2(k)]+f_{\pm}^2(k)}. \tag{23}$$

It follows from this expression that $b_1^{(\pm)}(k)$ changes its sign together with the function $\sin k\mp|f_{\pm}(k)|$. On the other hand, from Eq. (20) we calculate that the sign of $b_1^{(\pm)}$ determines whether the shock occurs in the front part of the dark $[a_{\pm}(k)<0]$ wave $[b_1^{(\pm)}(k)>0]$, when the parts of the wave characterized by larger $|a_{\pm}(k)|$ display higher velocity, or in the rear of the dark wave $[b_1^{(\pm)}(k)>0]$. Applying these arguments to the situation depicted in Fig. 9 one finds $\pm b_1^{(\pm)}<0$, in complete agreement with the numerical results. It is also of interest to remark that some features of the more involved phenomenon reported in Figs. 12 and 13 can be explained on the basis of Eq. (20). Indeed, as long as dark and bright waves are characterized by positive and negative values of $a_{\pm}$, it follows from Eqs. (20) and (23) that being excited at one point, the bright and dark shock waves move towards opposite directions with respect to the characteristic $n=V_{\pm}t$. Since, however, the speed of the relative motion is proportional to the amplitude, it is a small parameter and that is why the separation of the pulses occurs slowly. A confirmation that these arguments are indeed applicable to the case depicted in Fig. 12 follows from the fact that $f_{-}(\pi/6)>0$ and hence, taking into account the negative velocity of the motion, the bright shock must be more rapid than the dark one, i.e., exactly what one sees in Fig. 12. Finally, our numerical experiments clearly show that moving in the parameter space along the curves (11) towards the integrable limit $\epsilon=1$, the background radiation is always reduced and disappears at $\epsilon=1$ where the shock wave ''dissolves'' into a soliton's train. This agrees with our analytical prediction in Sec. II B, i.e., that shock waves in the DH limit should not exist.

V. CONCLUSION

In this paper we have shown that under suitable conditions bright and dark shock waves exist in the GDNLS on oscillating backgrounds of arbitrary wave number k. The methods used to characterize these waves, i.e., the linear analysis and the small-amplitude multiscale expansion, suggest that similar phenomena exist also in other DNLS-like systems with different types of nonlinearities and dispersion.

ACKNOWLEDGMENTS

V.V.K. acknowledges support from FEDER and Program PRAXIS XXI, Grant No. PRAXIS/2/2.1/FIS/176/94. M.S. acknowledges financial support from the Istituto Nazionale di Fisica della Materia and INTAS Grant No. 93-1324.

[1] M. Salerno, Phys. Rev. A **46**, 6856 (1992).
[2] M. Salerno, Phys. Lett. A **162**, 381 (1992).
[3] V. Z. Enol'skii, M. Salerno, A. C. Scott, and J. C. Eilbeck, Physica D **59**, 1 (1992).
[4] D. Cai, A. R. Bishop, and N. Gronbech-Jensen, Phys. Rev. Lett. **72**, 591 (1994).
[5] V. V. Konotop and S. Takeno, Phys. Rev. E **54**, 2010 (1996).
[6] Y. Xiao and W.-H. Hai, Phys. Lett. A **209**, 99 (1995).
[7] V. V. Konotop and S. Takeno, Phys. Rev. B **55**, 11 342 (1997).
[8] M. J. Ablowitz and J. F. Ladik, J. Math. Phys. **16**, 598 (1975).
[9] Yu. S. Kivshar and M. Salerno, Phys. Rev. E **49**, 3543 (1994).
[10] V. V. Konotop, O. A. Chubykalo, and L. Vázquez, Phys. Rev. E **48**, 563 (1993).
[11] D. Cai, A. R. Bishop, N. Gronbech-Jensen, and M. Salerno, Phys. Rev. Lett. **74**, 1186 (1995).
[12] D. Hennig, K. O. Rasmussen, G. P. Tsironis, and H. Gabriel, Phys. Rev. E **52**, R4628 (1995).
[13] V. V. Konotop and M. Salerno, Phys. Rev. E **55**, 4706 (1997).
[14] B. L. Holian and G. K. Straub, Phys. Rev. B **18**, 1593 (1978).
[15] B. L. Holian, H. Flaska, and D. W. McLaughlin, Phys. Rev. A **24**, 2595 (1981).
[16] D. J. Kaup, Physica D **25**, 361 (1987).
[17] S. Kamvissis, Physica D **65**, 242 (1993).
[18] J. Hietarinta, T. Kuusela, and B. A. Malomed, J. Phys. A **28**, 3015 (1995).
[19] P. Poggi, S. Ruffo, and H. Kantz, Phys. Rev. E **52**, 307 (1995).
[20] G. B. Whitham, *Linear and Nonlinear Waves* (Wiley, New York, 1974).
[21] K. Porsezian and M. Lakshman, Inverse Probl. **5**, L15 (1989).
[22] V. V. Konotop and M. Salerno (unpublished).
[23] V. V. Konotop, Phys. Rev. E **53**, 2843 (1996).